Ordering and segregation of a $Cu_{75}Pt_{25}(111)$ surface: A first-principles cluster expansion study

Koretaka Yuge, Atsuto Seko, Akihide Kuwabara, Fumiyasu Oba, and Isao Tanaka
Department of Materials Science and Engineering, Kyoto University, Sakyo, Kyoto 606-8501, Japan
(Received 30 January 2007; revised manuscript received 23 April 2007; published 12 July 2007)

Configurational thermodynamics for $Cu_{75}Pt_{25}$ (111) surfaces is examined by a first-principles calculation in conjunction with the cluster-expansion technique. The calculated surface segregation profile just below the bulk order-disorder transition temperature exhibits Pt segregation to the top and the third layers and Cu segregation to the second layer. No long-range ordered structure is found at the top layer. However, the simulated short-range-order parameter shows a small negative value, indicating a weak ordering tendency at the $Cu_{75}Pt_{25}$ alloy surface. This fact can be interpreted by the competition between the layer-confined spontaneous $p(2\times2)$ ordering tendency and the Pt segregation and interlayer surface ordering, which certainly disrupts the $p(2\times2)$ ordering. Five possible surface ground-state structures are found for the bulk $L1_2$ structure. The surface ground-state structures exhibit strongly localized electronic states composed of Pt and Cu *d* states at the topmost layer around 3 eV below the Fermi energy, which is consistent with the previous ultraviolet photoelectron spectroscopy measurement. One of the surface ground-state structures possesses additional surface states just below and above the Fermi energy, which are composed of Pt *d* states at the topmost layer. A significant ordering effect on the surface electronic states is confirmed for the $Cu_{75}Pt_{25}$ alloy.

DOI: 10.1103/PhysRevB.76.045407 PACS number(s): 81.30.−t, 68.35.Rh, 68.35.Md, 73.20.At

I. INTRODUCTION

It is widely known that the catalytic properties of transition-metal surfaces are significantly enhanced upon alloying with other metals.[1–4] The effects of alloying on their surface properties such as composition and atomic structure have therefore been one of the most attractive subjects in theoretical as well as experimental investigations. However, the atomic structure and composition profile of alloy surfaces sometimes depends strongly on sample preparation conditions, which makes it difficult to determine the thermodynamic equilibrium by measurements. Furthermore, another difficulty results from the fact that since atoms at the surface are in an anisotropic circumstance due to the termination of the crystal, bulk thermodynamic data cannot be simply applied to predict the behavior of the surface. It is therefore highly desirable to obtain a reliable prediction of the surface phase equilibria upon alloying to design and control the surface catalytic properties from a fundamental point of view.

The recent progress in computational techniques allows us to predict surface properties accurately based on density functional theory (DFT). However, when a problem requires the treatment of a large number of atoms or their configurations, the direct application of DFT requires a tremendous amount of computational effort. Important examples of problems regarding alloy surfaces are segregation behavior and the atomic-ordering tendency at a finite temperature, which typically require the consideration of millions of configuration spaces to produce a statistical ensemble average. To overcome such problems through DFT, an effective approach has been developed, which is called a "cluster expansion" (CE) technique.[5,6] Recent applications of the CE technique to the prediction of alloy-surface phase equilibria have been proved to be reliable and accurate.[7–9] This technique allows us to consider the energetics of millions of atomic arrangements within a few CPU hours on a standard PC, instead of considering a few specific arrangements directly via DFT calculations.

In this article, we discuss $Cu_{75}Pt_{25}(111)$ alloy surfaces based on the combination of first-principles calculations and CE. These surfaces have been considered as an interesting and important example in catalytic fields because they are more active catalysts for the oxidation of CO to CO_2 than pure Pt,[10–13] although Cu itself is less active than Pt. Therefore, several experimental and theoretical investigations have been devoted to examining the surface composition profile and atomic arrangements by various methods including low-energy electron diffraction (LEED), low-energy ion scattering (LEIS), auger electron spectroscopy (AES), ultraviolet photoelectron spectroscopy (UPS), and a tight-binding ising model (TBIM).[14–21] An ordered $Cu_{75}Pt_{25}(111)$ surface was successfully prepared by Schneider *et al.*[15–17] They obtained a LEED $p(2\times2)$ superstructure, which is the same pattern as that of the bulk $L1_2$ termination, with a slightly Pt-rich composition (30 at. % Pt), by annealing a sample slightly below the bulk order-disorder transition temperature $T=850$ K. However, subsequent experiments to determine the surface composition profiles under similar preparation conditions consistently resulted in LEED patterns of $p(1\times1)$ ordering, indicating no long-range ordering at this surface.[18–20] Direct observation of the topmost surface layer by scanning tunneling microscopy (STM) was reported by Mathauser and Teplyakov,[21] which shows the coexistence of 80% disordered and 20% $p(2\times2)$-ordered alloys. The distinct discrepancy in the observed atomic arrangements at this surface can be attributed to the sensitivity to the sample preparation conditions. Thus, up to now, an extensive discussion of the layer-resolved atomic arrangements under equilibrium conditions has not been performed. Not only the atomic arrangements, but also the surface composition profile appear to markedly vary under similar preparation conditions; Shen *et al.*[18] performed LIES and LEED measurements of the surface annealed at $T=850$ K, and found Cu segregation to the top layer and Pt segregation to the second layer. Gauthier *et al.*[20] performed a LEED measurement for the sample annealed at

$T=800-820$ K, to obtain the opposite segregation behavior: Pt segregation to the top and Cu segregation to the second layer. Moreover, the decay of elemental segregation with respect to the layer toward the bulk composition was shown to be much slower than that obtained by Shen *et al.*

Thus, the atomic arrangements including the ordering tendency and even the composition profile under equilibrium conditions for the $Cu_{75}Pt_{25}(111)$ surface below the bulk order-disorder transition temperature are still under discussion. In the present work, we report first-principles calculations on the segregation behavior, ordering tendency, and the possible ground-state atomic configurations of the surface and its electronic structure for the bulk $L1_2$-ordered phase, in conjunction with the CE technique. The effects of a finite temperature on the atomic configuration are considered using canonical and grand-canonical Monte Carlo (MC) simulations based on effective cluster interactions (ECIs) obtained from the CE.

II. METHODOLOGY

The CE technique is adopted to expand DFT energies at given atomic configurations. The details of the present bulk and surface CE formalisms are described in Ref. 9. In simple terms, two basis functions of 1 (unity) and σ for each lattice point are used to construct cluster functions, where $\sigma_i=+1$ is adopted to represent Pt occupation in lattice site i, and $\sigma_i=-1$ represents Cu occupation. Note that one important feature specific to the surface CE is that surface ECIs in sufficiently deep layers should approach their corresponding bulk values. Therefore, in DFT total-energy calculations, surface layers should be sufficiently thick for the ECIs of the middle layers to become bulklike.

To determine the ECIs, we perform a least-squares (LS) fitting of the total energies for ordered structures obtained through a first-principles technique. The first-principles calculations are carried out using a DFT code, the Vienna *Ab-initio* Simulation Package (VASP).[22–24] All-electron Kohn-Sham equations are solved by employing the projector augmented-wave (PAW) method,[25] within the local-density approximation (LDA) to an exchange-correlation functional.[26,27] A plane-wave cutoff energy of 360 eV is used throughout the calculations. We obtain total energies for 36 bulk ordered structures, all consisting of 32 atoms, i.e., a $2\times2\times2$ expansion of the fcc unit-cell. Brillouin zone integration is performed on the basis of the Monkhorst-Pack scheme[28] with an $8\times8\times8$ k-point mesh. Geometry optimization is performed until the residual forces become less than 1 meV/Å. In the case of the surfaces, total-energy calculations for 95 ordered slabs are performed. For the $Cu_{75}Pt_{25}(111)$ surfaces, we find that a nine-layer slab is sufficient to achieve the convergence of surface ECIs to nearly bulk values. These slabs consist of 36, 54, and 72 atoms, i.e., $2\times2\times9$-layer, $2\times3\times9$-layer, and $2\times4\times9$-layer slabs, respectively. The vacuum region is taken to be 16 Å. During the geometry optimization, the in-plane lattice parameters of the slabs are fixed to an optimized theoretical value of 3.64 Å to mimic the strain induced by the $Cu_{75}Pt_{25}$-ordered alloy. Through this optimization, the corresponding surface ECIs automatically include the surface relaxation effect under a suitable epitaxial strain induced by the bulk. Brillouin zone integration is performed on a $6\times6\times1$ k-point mesh for the (2×2) surface slabs, and on smaller meshes with same spacings for the larger slabs.

For the practical use of the cluster expansion, we cannot include an infinite number of ECIs because of the limitation on the number of DFT input energies. Therefore, we should choose an optimal set of a finite number of clusters so that the fitting error becomes as small as possible. A cross-validation (CV) score,[29,30] ξ, can be a satisfactory criterion for estimating the uncertainty of the energies predicted by ECIs. To minimize the CV score, we adopt the genetic algorithm (GA),[31,32] where the information of candidate clusters is lined up as genetic information. In the present work, the mutation rate and population size are set to be 0.05 and 20, respectively.

Careful attention must be paid not only to the choice of clusters, but also to the selection of DFT input structures. Although the CV score can give a prediction power of energies for a given set of structures, this does not tell us which structures are energetically important in problems of interest. In the present case, our interests are directed mainly to the ground-state properties and their related disordered states of the surface. We therefore select DFT input structures based on the construction of ground-state lines.[33] In this ansatz, there are several steps to determine the optimal input structures: (i) DFT total-energy calculations for randomly selected structures are performed. (ii) GA is applied to find an optimal set of clusters and their ECIs. (iii) Using the ECIs, ground-state lines are constructed. (iv) If the structures on or near the ground-state lines are not included in the DFT input structures, add these structures. Steps (i) to (iv) are repeated until the ground-state lines and the input structures are consistent. This procedure can be efficient for determining the optimal set of input structures and clusters for both the bulk and the surface, except for the case that different bulk concentrations are considered together.[9]

Finite-temperature thermodynamic properties are evaluated using canonical and grand-canonical MC simulations with the Metropolis algorithm.[34] For the bulk MC simulation box, an $8\times8\times8$ expansion of the fcc unit cell is found to be sufficient for our discussion in terms of the finite size effect. Similarly, we use $12\times12\times9$-layer slabs for the surface MC simulation. 5000 MC steps per site are performed for equilibration, followed by 2000 steps per site for sampling at each temperature and composition. In each sampling step, the total energy of the system, atomic positions, and ordering parameters are stored to obtain statistical averages.

III. RESULTS AND DISCUSSION

A. Effective interactions for bulk and surface $Cu_{75}Pt_{25}$ alloys

Following the procedure described in Sec. II, an optimal set of bulk clusters is selected as shown in Fig. 1. We determined 7 clusters from the 53 clusters up to quadraplet that are possible within the maximum distance of constituent pairs up to the fourth nearest neighbor (NN) of the fcc lattice. The seven clusters consist of an empty cluster, a point, two

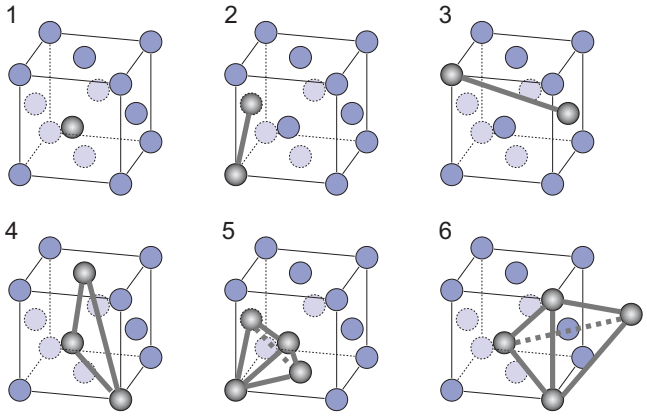

FIG. 1. (Color online) Optimal set of selected clusters for the bulk Cu-Pt alloy obtained by minimizing the CV score using GA.

pairs, a triplet, and two quadruplets. The set of clusters gives a CV score of 3.8 meV/atom, which is sufficiently accurate to express the relative bulk energetics. The corresponding ECIs are shown in Fig. 2. The dominant contributions of the two pairs both show a positive sign, indicating a preference for unlike-atom pairs for the first and third NN coordination.

Applying these ECIs to the canonical MC simulation, we estimated the bulk order-disorder transition temperature T_c. A disordered $Cu_{75}Pt_{25}$ alloy is found to undergo a phase transition into the $L1_2$-ordered alloy at around $T_c=900$ K, confirmed by the singularity of the simulated specific heat. This result is comparable to the early experimental reports of $T_c \sim 870$ K for the transition from disorder to the $L1_{2-s}$-ordered structure.[35–37] Here, $L1_{2-s}$ is a one-dimensional long-period superlattice (LPS), which is interpreted to be the antiphase domain structures of the $L1_2$ structure with a long period $2M \sim 14$. The $L1_{2-s}$ LPS is reported to transform into the $L1_2$ structure at around 790 K. We do not consider the effect of the existence of the $L1_{2-s}$ LPS on the surface state, since such a long-period ordering effect on surface segregation and atomic arrangement is beyond the scope of this work. The

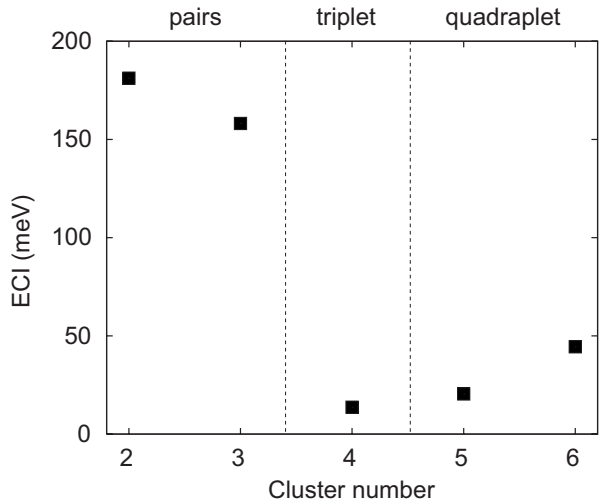

FIG. 2. Fitted ECIs for the bulk Cu-Pt alloy. The abscissa represents the cluster numbers shown in Fig. 1.

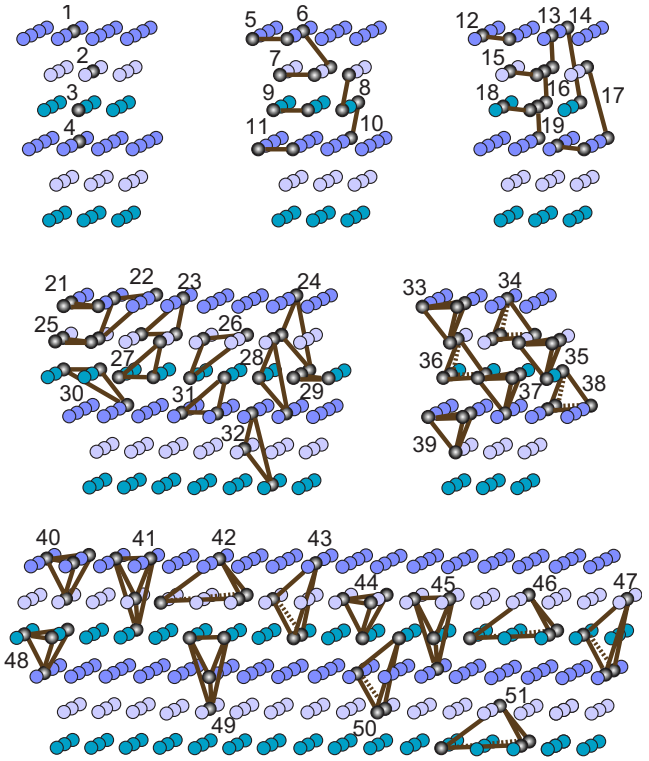

FIG. 3. (Color online) Clusters for the $Cu_{75}Pt_{25}(111)$ surface.

reasons for neglecting the existence of the LPS are threefold as follows: (i) Since the LPS retains the $L1_2$ structure for a long period of $M \sim 7$, this should not significantly affect the surface atomic ordering tendency within moderate atomic distances, nor should it affect the surface segregation. (ii) For in-plane lattice parameters, that can significantly affect the surface segregation, the difference between the $L1_2$ and $L1_{2-s}$ structures is almost negligible because the average lattice parameter of the $L1_{2-s}$ LPS differs only by 0.1% from that of the $L1_2$ structure, and even the axial ratio c/a differs only by 0.004.[38] (iii) The ground-state surface structures at $T=0$ K can be considered on the basis of the bulk $L1_2$ structure, because the $Cu_{75}Pt_{25}$ alloy in the lower-temperature side certainly exhibits the $L1_2$ structure. Therefore, we consider that the surface state together with the bulk $L1_2$ structure becomes an important and fundamental start in essentially understanding the segregation behavior and atomic arrangements for $Cu_{75}Pt_{25}$ alloy surfaces below the bulk order-disorder transition temperature.

Once the bulk clusters to be used in the CE are obtained, the corresponding surface clusters can be automatically determined. Since the surface clusters should be layer dependent, the above seven bulk clusters are now split into 52 surface clusters in the present nine-layer slab model, which are shown in Fig. 3. The corresponding CV score is estimated to be 4.0 meV/atom. These clusters can be separately divided into 6 parts with respect to their dimension n and type f. In each dimension and type of cluster, the cluster numbers are assigned so that clusters in the deeper layer have as large numbers as possible. The respective fitted ECIs are given in Fig. 4. The vertical dotted lines segment the clusters

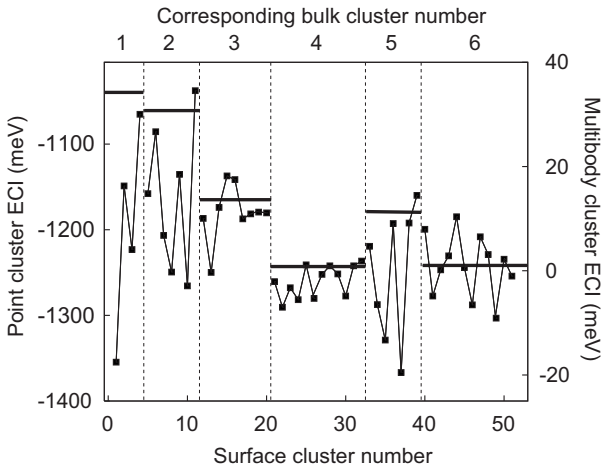

FIG. 4. Fitted ECIs per cluster for the $Cu_{75}Pt_{25}(111)$ surface. The horizontal bars represent the corresponding bulk ECIs.

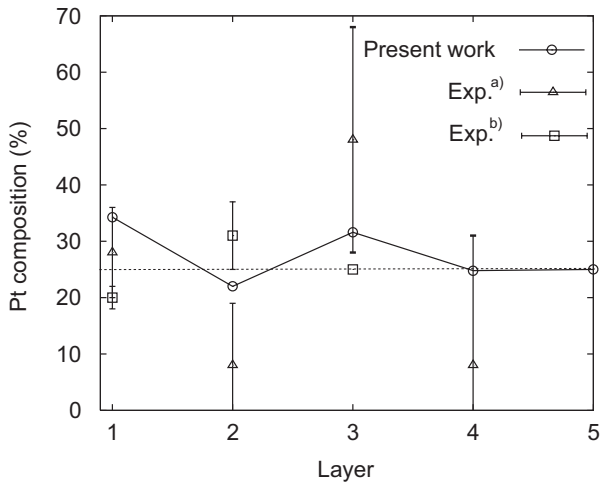

FIG. 5. Surface composition profile of Pt for the $Cu_{75}Pt_{25}(111)$ surface. Open circles denote the results from the present MC simulation (T=800 K). Open triangles, LEED study (T=800–820 K) (Ref. 20); open squares, LEED study (T=850 K) (Ref. 18).

in a similar fashion to Fig. 3, where the corresponding cluster numbers for the bulk shown in Fig. 1 are given together on the upper side of the abscissa. The horizontal bars represent the bulk ECIs for the clusters described on the upper abscissa. It can be seen from Fig. 4 that all the surface ECIs for the middle layers, i.e., deeper than the fourth layer, satisfactorily approach the corresponding bulk values, indicating the convergence of the surface ECIs with respect to the layer. The greater negative values of all the surface point cluster ECIs with respect to the corresponding bulk value, represented by the leftmost segment in Fig. 4, imply Pt segregation to the respective layers. However, the quantitative estimation of segregation demands the consideration of the effect of atomic ordering, as described by the balance with the other ECIs, which is discussed in the following section.

B. Segregation and ordering at $Cu_{75}Pt_{25}(111)$ surfaces

Applying the above 52 surface ECIs to the grand-canonical MC simulation, we estimated the surface composition profile below the estimated bulk order-disorder transition temperature T=800 K. The result is shown in Fig. 5 together with those from early experimental reports.[18,20]

The present result shows oscillating segregation behavior with Pt-rich layers at the top and the third layers and a Cu-rich layer at the second layer. A particularly significant contribution of the ordering effect to the segregation can be seen at the second layer, which results in a reversal Cu segregation despite an on-site energy gain in Pt segregation, as expected from the negative ECI for the point cluster shown in Fig. 4. This is in contrast to the segregation at Pt-Rh(111) surfaces, where Pt enrichment and depletion at the top and second layers are virtually determined by the negative and positive on-site Pt segregation energies at the respective layers.[9] The dominant contribution of the on-site segregation energy results from the weak ordering tendency of the Pt-Rh surfaces, which should typically be related to the low bulk order-disorder transition temperature of $T \sim 100$ K. However, the $Cu_{75}Pt_{25}$ alloy exhibits a rather high bulk order-disorder transition temperature of $T \sim 900$ K, which reflects the non-negligible order of multibody surface ECIs compared with on-site surface segregation energies, as shown in Fig. 4. Thus, the segregation at the $Cu_{75}Pt_{25}(111)$ surface is determined by a complicated competition between the segregation energies and the ordering tendency at respective layers, which cannot be simply interpreted as being similar to the Pt-Rh case.

The simulated segregation exhibits a similar tendency to the experimental results in Ref. 20, and opposite to those in Ref. 18. However, compared with Ref. 20, the present simulation shows a relatively weak amplitude of oscillation and rapid convergence in composition toward the bulk value as being away from the surface. The convergence in the simulated composition at the fourth layer can be clearly related to the approach of surface ECIs to the bulk values at the fourth layer, as described in the previous section.

No long-range ordered structure is found at the simulated Pt-rich top layer, while a short-range ordering tendency is recognized. The ordering tendency at the top layer is quantitatively evaluated using the Warren-Cowley short-range order (SRO) parameter,[39] which is given by

$$\alpha_j = 1 - \frac{P_{AB}^j}{2x_A x_B}, \tag{1}$$

where P_{AB}^j denotes the probability of finding an A-B unlike atomic pair in type j, and x_A and x_B denote the compositions of elements A and B, respectively. The simulated SRO parameter for the first NN pair at the top layer, $\alpha_{1\mathrm{NN}}$, is estimated to be −0.18. The negative sign indicates an ordering tendency at this surface. This result is in agreement with early measurements using K^+ ion scattering, which confirmed that the Pt atoms at the top layer are not clustered.[18,19] To investigate the origin of this short-range ordering at the top layer, we searched for the top-layer configuration with the lowest total energy for the bulk stoichiometric composition of $Cu_{75}Pt_{25}$ through canonical MC simulations with only

top-layer-confined surface ECIs. The simulation results in a $p(2\times2)$ superstructure, which is identical to the ideal bulk $L1_2$ termination. These facts indicate that the short-range ordering at the top layer can be interpreted by the competition between the layer-confined spontaneous $p(2\times2)$ ordering tendency and the Pt segregation and interlayer surface ordering effects, which certainly disrupt the $p(2\times2)$ ordering.

In contrast to the top layer, the fourth and fifth layers exhibit the $L1_2$-ordered structure below the bulk order-disorder transition temperature. Therefore, the fourth layer achieves a bulklike state in terms of both composition and atomic arrangement, which can also be predicted by the convergence of the surface ECIs shown in Fig. 4.

C. Surface ground states for bulk $L1_2$-ordered structure

Since the atomic ordering and composition profile at the $Cu_{75}Pt_{25}$ surfaces are considered to be sensitive to sample preparation conditions,[15,18,20] listing the possible surface ground-state configurations becomes an important task in providing an experimental interpretation of fundamental information on the atomic arrangements. Following the previous section, consideration of the top three layers could now be sufficient to determine the atomic arrangements specific to the surface. Therefore, the surface-specific atomic arrangements γ can be examined on the bulk $L1_2$-ordered structure in terms of surface mixing enthalpy, defined as

$$\Delta E_{\mathrm{surf}}^{\mathrm{mix}}(\gamma) = E_{\mathrm{surf}}(\gamma/L1_2) - x_{\mathrm{Pt}}E_{\mathrm{surf}}(\mathrm{Pt\ 3L}/L1_2) - (1-x_{\mathrm{Pt}})E_{\mathrm{surf}}(\mathrm{Cu\ 3L}/L1_2), \quad (2)$$

where E_{surf} denotes the surface energy, x_{Pt} is the Pt composition at the top three layers, and $\gamma/L1_2$, Pt $3\mathrm{L}/L1_2$, and Cu $3\mathrm{L}/L1_2$ are the configuration γ, three-layer Pt, and three-layer Cu on the $L1_2$ structure, respectively. Therefore, the surface mixing enthalpy $\Delta E_{\mathrm{surf}}^{\mathrm{mix}}(\gamma)$ represents the surface energy for a configuration γ on the $L1_2$ structure with respect to three-layer Pt and Cu on $L1_2$ as reference energies.

In the present study, the energies for all the possible configurations consisting of up to 24 atoms in the surface region on a surface concentration grid with intervals of 8.33% are predicted using the surface ECIs. The resultant surface mixing enthalpies are shown in Fig. 6. The negative surface mixing enthalpies for the possible structures can certainly be attributed to the significant positive sign of ECIs for surface-pair clusters, as shown in Fig. 4. Five ground-state atomic arrangements, represented by the large filled circles, are possible for this surface when the surface composition is given. Our interest is mostly directed to the ground states at x_{Pt}

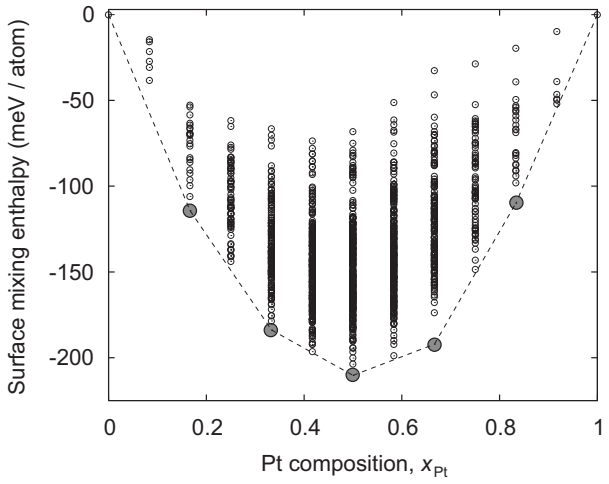

FIG. 6. Ground-state convex hull for the top three layer atomic arrangements of the top three layers on $L1_2$ as a function of surface Pt composition x_{Pt}. A total of five ground-state atomic arrangements are recognized, as represented by the large filled circles.

$=0.167$ and 0.33, since the observed average Pt composition for both ordered and disordered surfaces in the first several layers typically ranges between these values.[17,18,20,21] These ground states are described schematically in Table I, where filled circles denote Cu atoms and open circles represent Pt. For $x_{\mathrm{Pt}}=0.167$, the layer stacking is $p(2\times2)$, Cu $1L$, and $p(2\times2)$, while for $x_{\mathrm{Pt}}=0.33$, it is $p(2\times1)$, Cu $1L$, and $p(2\times1)$. In particular, the type I structure with $p(2\times2)$ ordering is consistent with the observed $Cu_{75}Pt_{25}$ surface ordered structure, which exhibits a $p(2\times2)$ LEED pattern.[16] We investigated not only the atomic arrangements, but also the surface atomic relaxation for the type I and II structures through DFT total-energy calculations. The resultant average interlayer distances between the ith and jth layers measured from the bulk value Δd_{ij} and the layer Pt compositions C_i are summarized in Table II together with those from an early experimental report.[20] A qualitative similarity of the contraction can be seen between the second and third layers, and expansion between the third and fourth interlayer distances for type I and II structures, and the experimental results.

The atomic arrangements for the surface compositions between $x_{\mathrm{Pt}}=0.167$ and 0.33 are always in a two-phase region consisting of types I and II. Therefore, hereinafter, we discuss these two ordering types as representative structures in order to interpret the surface electronic state on the bulk $L1_2$ structure.

TABLE I. Schematic illustration of the surface ground-state configurations viewed along the normal to the (111) plane. Filled circles denote Cu atoms and open circles represent Pt atoms.

Type	x_{Pt}	Top layer	2nd layer	3rd layer
I	0.167			
II	0.33			

TABLE II. Layer Pt composition C_i and the interlayer distance measured from the bulk value Δd_{ij}.

C_i, Δd_{ij} (Å)	Type I	Type II	Exp.[a]
C_1	0.25	0.5	0.28±0.08
C_2	0	0	0.08±0.11
C_3	0.25	0.5	0.48±0.20
C_4	0.25	0.25	0.08±0.23
Δd_{12}	−0.05	−0.01	+0.006±0.01
Δd_{23}	−0.03	−0.01	−0.004±0.02
Δd_{34}	+0.01	+0.03	+0.046±0.02

[a]Reference 20: LEED study at $T=800-820$ K.

D. Surface electronic structures

Figure 7 shows the calculated projected electronic density of states (PDOS) at the top layer for types I and II, where the solid curves represent the Pt contribution, and dashed curves represent Cu. Only the *d*-state contributions are drawn, since other orbitals provide an insignificant contribution to the total DOS in this energy range. The calculated PDOS for the bulk $L1_2$ structure and a reported UPS for the $p(2\times2)$-ordered surface[17] are displayed together. In the UPS, features around −0.9 and −4.0 eV relative to the Fermi energy are Pt induced, that at −2.4 eV is Cu induced, while that at −3.0 eV is from the superposition of the Cu and Pt states.

The DOS for bulk $L1_2$ is dominated by the peak at −4.6 eV from both Pt and Cu, at −2.9 and −2.2 eV mainly from Cu, at −1.6 eV from Cu, and −1.6 to −1.0 eV mainly from Pt. For the DOS at the top layer for the type I and II structures, a pronounced difference from the bulk DOS can be recognized both for the Pt and Cu contributions. The dominant peaks at −4.6 and −1.6 eV for the bulk $L1_2$ Cu DOS are significantly weakened for type II, and almost disappear for type I. The other two dominant peaks for bulk retain their features at both surfaces. For the Pt DOS at the surfaces, three distinct features can be seen. (i) The peak at −4.6 eV for bulk $L1_2$ moves toward a higher energy by ~0.6 eV for both type I and type II. This can be related to the *d*-band narrowing at the surfaces due to a decrease in the second moment of DOS resulting from a lower coordination number at the surface, in terms of a simple NN tight-binding model.[40] However, the calculated bandwidth narrowing is slightly weaker than the predicted reduction by a factor of $\sqrt{9/12}$, derived from the fact that the bandwidth is proportional to the square root of the coordination number. Consequently, the calculated peak is moved to −4.0 eV for both types, which is comparable to the observed Pt-related peak at −4.0 eV shown in Fig. 7(d). (ii) Sharp peaks relative to the bulk one are recognized around −1.0 eV for both surfaces, which could be associated with the observed Pt-related peak at −1.0 eV, while an extra peak slightly below the Fermi energy also appears for the type II surface. (iii) A significant increase in the peak intensity at around −3.0 eV for both surfaces can be seen, compared with the peak for bulk $L1_2$ at around the same energy. We also found that the increase in the intensity for this peak is confined to the topmost-layer

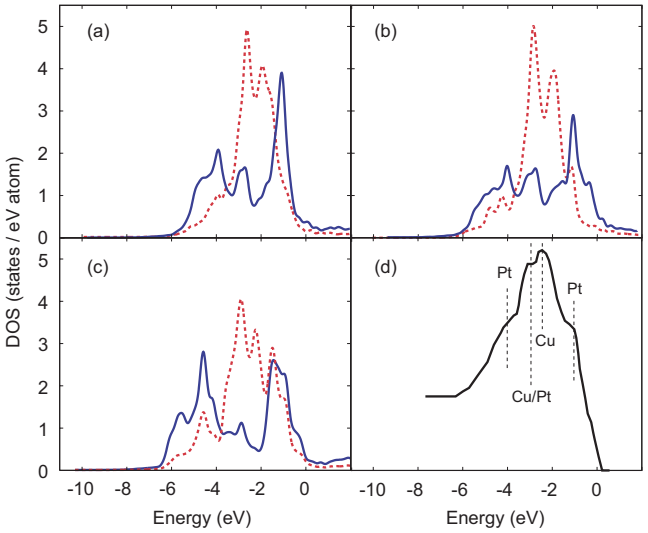

FIG. 7. (Color online) Projected electronic density of states (PDOS) of *d*-state contribution at the top layer for the (a) type I structure, (b) type II structure, (c) bulk $L1_2$ structure, and (d) UPS for the $p(2\times2)$ ordered surface. (Reference 17) (a)–(c): Dotted curves represent the Cu contribution, and the solid curves represent Pt. Energies are measured from the Fermi level.

DOS, and is markedly reduced at subsurface layers for both surfaces.

A more detailed analysis on the surface electronic structure is performed using surface-band structures. Figure 8 shows the calculated electronic-band dispersions for the type I and II surfaces along the high symmetry points of the underlying 2D Brillouin zone of the fcc (111) surface. Electronic states containing more than 80% of the contribution of the topmost layer are considered to be strongly localized surface states, which are represented by filled circles in Fig. 8; more than 60% weakly localized surface states represented by open circles. We found that almost all the surface states basically consist of significant *d*-state contributions. Many number of strongly as well as weakly localized surface states can be seen around the energy of −3.0 eV and near the $\bar{K}$ and $\bar{M}$ points both for type I and II surfaces. From the analysis of the orbital and site decomposition at each *k* point, these states are found to be dominated by the Pt and Cu *d* states at the top layer for both type I and II surfaces. These features correspond to the strong peaks found at around −3.0 eV for the Pt and Cu *d* states relative to the bulk one shown in Fig. 7, which could correspond to the observed peak at −3.0 eV of the Cu and Pt superposition shown in Fig. 7(d). Another important point regarding the surface band structures is that additional strongly localized surface states are found for type II, particularly along the $\bar{\Gamma}\bar{M}$ direction around the Fermi energy, while this does not hold for type I. We have confirmed that the surface states around the Fermi energy for the type II surface are dominated by the top-layer Pt *d* state, which is associated with the formation of the extra peak just below the Fermi energy in its DOS from the Pt contribution, as shown in Fig. 7(b).

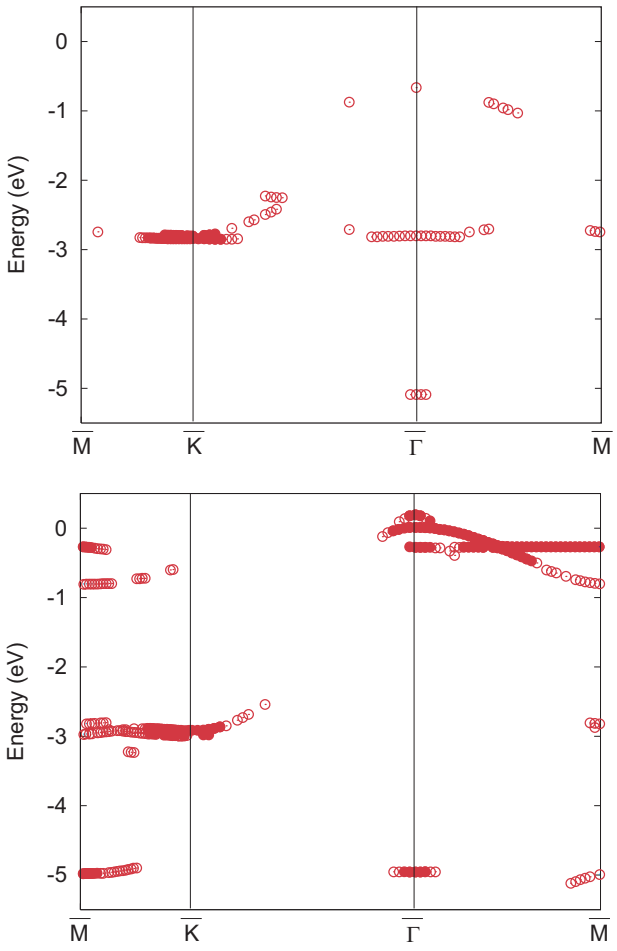

FIG. 8. (Color online) Surface-band structure for the type I (upper figure) and type II (lower figure) ordered structures. The Fermi energy is set at 0 eV. The plots are along the same direction, with indicated symmetry points referring to the underlying fcc (111) surface 2D Brillouin zone. The filled and open circles represent strongly and weakly localized surface states containing more than 80 and 60 % contributions of the top layer, respectively.

IV. CONCLUSIONS

Configurational thermodynamics of $Cu_{75}Pt_{25}(111)$ surfaces was investigated by considering the combinations of the cluster expansion and first-principles calculations. The segregation behavior just below the bulk order-disorder transition temperature was examined by MC simulations with surface ECIs. We found that Pt segregates to the top and the third layers, while Cu segregates to the second layer. No long-range ordered structure was found at the topmost layer, while the short-range-order parameter exhibits a negative sign, which indicates that a weak ordering tendency still remains at the top layer. This ordering behavior can be interpreted by the competition between the spontaneous $p(2\times2)$ ordering tendency at the top layer and the Pt segregation and interlayer-ordering tendency. The behavior of the top three layers was found to be sufficient to describe the surface-specific state in terms of both composition and atomic arrangements. Surface ground-state atomic arrangements for the bulk $L1_2$-ordered structure were investigated in terms of the surface mixing enthalpy. Two important surface ground states were found at the surface compositions of 0.167 (type I) and 0.33 (type II). The type I surface possesses $p(2\times2)$ ordering at the topmost layer, which is consistent with the previously observed $Cu_{75}Pt_{25}$-ordered surface with a $p(2\times2)$ LEED pattern. The electronic structure of the $Cu_{75}Pt_{25}(111)$ type I and II surfaces was examined using the DOS and band structure, and compared with the reported UPS. For both type I and II surfaces, the top layer shows a significant peak at around −3.0 eV relative to the Fermi energy in the DOS, which is dominated by the surface-confined Pt and Cu *d* states. This result is comparable to the observed UPS peak at −3.0 eV, which was interpreted by the superposition of the Pt and Cu contributions. The type II surface has additional significant surface states around the Fermi energy, which are dominated by the Pt *d* states at the top layer. Significant ordering effects on the surface electronic states were thus confirmed for the $Cu_{75}Pt_{25}$ alloy. These results could be of great interest because the localization of surface electronic states on metals and their alloys can affect a variety of surface phenomena such as catalytic reactions.

ACKNOWLEDGMENT

This work was financially supported by the New Energy and Industrial Technology Development Organization (NEDO) of Japan.

[1] J. H. Sinfelt, Adv. Catal. **23**, 91 (1973).
[2] W. M. H. Sachtler and R. A. van Santen, Adv. Catal. **26**, 69 (1977).
[3] J. L. Carter, G. B. McVicker, W. Weissman, W. S. Kmak, and J. H. Sinfelt, Appl. Catal. **3**, 327 (1982).
[4] M. J. P. Botman, K. de Vreugd, H. W. Zandbergen, R. de Block, and V. Ponec, J. Catal. **116**, 467 (1989).
[5] J. M. Sanchez, F. Ducastelle, and D. Gratias, Physica A **128**, 334 (1984).
[6] D. de Fountain, *Solid State Physics*, edited by H. Ehrenreich and D. Turnbull (Academic Press, New York, 1994), Vol. 47, pp. 33–176.
[7] S. Müller, J. Phys.: Condens. Matter **15**, R1429 (2003).
[8] B. C. Han, A. Van der Ven, G. Ceder, and B. J. Hwang, Phys. Rev. B **72**, 205409 (2005).
[9] K. Yuge, A. Seko, A. Kuwabara, F. Oba, and I. Tanaka, Phys. Rev. B **74**, 174202 (2006).
[10] J. T. Kunmmer, J. Catal. **38**, 166 (1975).
[11] H. C. de Jonstec and V. Ponec, J. Catal. **63**, 389 (1980).
[12] U. Schneider, G. R. Castro, and K. Wandelt, Surf. Sci. **287/288**, 146 (1993).
[13] M. Kolodziejczyk, R. E. E. Colen, M. Berdau, B. Delmon, and J.

H. Block, Surf. Sci. **375**, 235 (1997).
[14] A. Senhaji, G. Tréglia, and B. Legrand, Surf. Sci. **307-309**, 440 (1994).
[15] G. R. Castro, U. Schneider, H. Busse, T. Janssens, and K. Wandelt, Surf. Sci. **269/270**, 321 (1992).
[16] U. Schneider, G. R. Castro, H. Busse, T. Janssens, J. Wesemann, and K. Wandelt, Surf. Sci. **269/270**, 316 (1992).
[17] U. Schneider, G. R. Castro, and K. Wandelt, Surf. Sci. **287/288**, 146 (1993).
[18] Y. G. Shen, D. J. O'Connor, R. J. MacDonald, and K. Wandelt, Solid State Commun. **96**, 557 (1995).
[19] Y. G. Shen, D. J. O'Connor, K. Wandelt, and R. J. MacDonald, Surf. Sci. **328**, 21 (1995).
[20] Y. Gauthier, A. Senhaji, B. Legrand, G. Tréglia, C. Becker, and K. Wandelt, Surf. Sci. **527**, 71 (2003).
[21] A. T. Mathauser and A. V. Teplyakov, Surf. Sci. **523**, 37 (2003).
[22] G. Kresse and J. Hafner, Phys. Rev. B **47**, R558 (1993).
[23] G. Kresse and J. Furthmüller, Phys. Rev. B **54**, 11169 (1996).
[24] G. Kresse and D. Joubert, Phys. Rev. B **59**, 1758 (1999).
[25] P. E. Blöchl, Phys. Rev. B **50**, 17 953 (1994).
[26] D. M. Ceperley and B. J. Alder, Phys. Rev. Lett. **45**, 566 (1980).
[27] J. P. Perdew and A. Zunger, Phys. Rev. B **23**, 5048 (1981).
[28] H. J. Monkhost and J. D. Pack, Phys. Rev. B **13**, 5188 (1976).
[29] M. Stone, J. R. Stat. Soc. Ser. B (Methodol.) **36**, 111 (1974).
[30] D. M. Allen, Technometrics **16**, 125 (1974).
[31] G. L. W. Hart, V. Blum, M. J. Walorski, and A. Zunger, Nat. Mater. **4**, 391 (2005).
[32] A. van de Walle, Nat. Mater. **4**, 362 (2005).
[33] V. Blum and A. Zunger, Phys. Rev. B **70**, 155108 (2004).
[34] N. Metropolis, A. W. Rosenbluth, M. N. Rosenbluth, A. H. Teller, and E. Teller, J. Chem. Phys. **21**, 1087 (1953).
[35] A. Rudnitskii, Zh. Neorg. Khim. **1**, 1305 (1956).
[36] L. R. Bidwell, W. J. Schulz, and R. K. Saxer, Acta Metall. **15**, 1143 (1967).
[37] S. Ogawa, H. Iwasaki, and A. Terada, J. Phys. Soc. Jpn. **34**, 384 (1973).
[38] K. Schubert, B. Kiefer, M. Wilkens, and R. Haufler, Z. Metallkd. **46**, 692 (1955).
[39] J. M. Cowley, J. Appl. Phys. **21**, 24 (1950).
[40] A. Zangwill, *Physics at Surfaces* (Cambridge University Press, Cambridge, 1988).